NeuroImage 84 (2014) 35–44

Contents lists available at ScienceDirect

NeuroImage

journal homepage: www.elsevier.com/locate/ynimg

Brain maturation of the adolescent rat cortex and striatum: Changes in volume and myelination

Luam Mengler [a], Artem Khmelinskii [b], Michael Diedenhofen [a], Chrystelle Po [a], Marius Staring [b], Boudewijn P.F. Lelieveldt [b,c], Mathias Hoehn [a,*]

[a] In-vivo-NMR Laboratory, Max Planck Institute for Neurological Research, Cologne, Germany
[b] Division of Image Processing, Dept. of Radiology, LUMC, Leiden, The Netherlands
[c] Dept. of Intelligent Systems, Delft University of Technology, Delft, The Netherlands

ARTICLE INFO

Article history:
Accepted 16 August 2013
Available online 27 August 2013

Keywords:
Brain development
Age-dependent T2 relaxation changes
Age-dependent diffusion changes
Myelination maturation
Tissue restructuring during cerebral development
Volume changes of cerebral structures during development

ABSTRACT

Longitudinal studies on brain pathology and assessment of therapeutic strategies rely on a fully mature adult brain to exclude confounds of cerebral developmental changes. Thus, knowledge about onset of adulthood is indispensable for discrimination of developmental phase and adulthood. We have performed a high-resolution longitudinal MRI study at 11.7 T of male Wistar rats between 21 days and six months of age, characterizing cerebral volume changes and tissue-specific myelination as a function of age. Cortical thickness reaches final value at 1 month, while volume increases of cortex, striatum and whole brain end only after two months. Myelin accretion is pronounced until the end of the third postnatal month. After this time, continuing myelination increases in cortex are still seen on histological analysis but are no longer reliably detectable with diffusion-weighted MRI due to parallel tissue restructuring processes. In conclusion, cerebral development continues over the first three months of age. This is of relevance for future studies on brain disease models which should not start before the end of month 3 to exclude serious confounds of continuing tissue development.

Introduction

Brain development is a continuous process, which proceeds well after birth and even adolescence. Most studies employing rats claim to use "young adults", implying a fully matured brain parenchyma. However, the definition for "young adults" is diverse and ranges between two and four months old and body weight of 200 to 350 g.

For longitudinal studies it is particularly important to be able to discriminate between natural, development-dependent tissue changes and those alterations due to induced diseases or lesions. As individual organs, tissues and microstructures mature at different paces, great care must be taken in choosing the age and observation period for the animal model of interest.

Adolescence is understood as the time of transition between infancy and adulthood, despite a lack of clear and unambiguous boundaries between those stadiums. In some cases, adulthood is used equivalent to full sexual maturity. Depending on the research interest, adolescence is described by changes not only in social (Meaney and Stewart, 1981), cognitive or risk-taking behavior (Spear and Brake, 1983), but also in the neurotransmitter system (Andersen, 2003). The onset and extent of this phase may differ for different strains/breeds, between the sexes and for further different parameters, and conservative age range includes postnatal days 28 to 42 (Spear, 2000). This time window starts about a week after rat's weaning age and ends shortly after sexual maturity.

As many of these characterizations were based on group comparisons at different ages, they describe mere group averaged values, while inter-individual variability in the temporal profile of development may be completely lost. We hypothesized that intra-individual longitudinal studies using noninvasive imaging modalities may allow the identification of biomarkers of developmental phases of the brain which will distinguish between an early, adolescent period of pronounced cerebral development and a later, matured, "steady state" cerebral adulthood. We further hypothesized that such biomarkers could be reflected either in anatomical, structural and volume changes over time or in quantitative tissue characterization through physiology-based imaging parameters. For this purpose, we have followed male Wistar rats from 21 days until 6 months. We measured whole brain, cortical and striatal volume changes with high-resolution T_2-weighted MRI to look for structure-related biomarkers. For developmental tissue changes, T_2 relaxometric

* Corresponding author at: In-vivo-NMR Laboratory, Max Planck Institute for Neurological Research, Gleuelerstrasse 50, D-50931 Köln, Germany. Fax: +49 221 4726 337.
E-mail address: mathias@nf.mpg.de (M. Hoehn).

1053-8119
http://dx.doi.org/10.1016/j.neuroimage.2013.08.034

imaging and diffusion imaging were recorded to investigate the microstructure of the tissue and the myelination, respectively.

Materials and methods

Animals

All animal experiments were conducted in accordance with the German Animal Welfare Act and approved by the local authorities (Landesamt für Naturschutz, Umwelt und Verbraucherschutz NRW). From postnatal day 21 on (weaning age) twelve male Wistar rats (Harlan-Winkelmann GmbH, Borchen, Germany, and Janvier, Le Genest Saint Isle, Cedex, France) were held in an environment with controlled temperature (21 +/− 1 °C), humidity (55%+/− 10%), and light (12/12 h dark/light cycle). Animals were housed in groups of four until the age of two months, and in pairs afterwards, and were given access to food and water *ad libitum*.

Study design

Animals were subdivided into three survival groups: three weeks (n = 4), three months (n = 4) and six months (n = 4) to obtain histological specimens of all those ages. MRI experiments were conducted at the age of three weeks (3W), one (1M), two (2M), three (3M) and six (6M) months, until sacrifice, depending on group. Hereafter, we will refer to these time points using the above-introduced abbreviations.

MRI

MRI experiments were conducted on an 11.7 T Bruker BioSpec horizontal bore, dedicated animal scanner (Bruker Biospin, Ettlingen, Germany). RF transmission was achieved with a quadrature volume resonator (inner diameter 72 mm), while a quadrature rat brain surface coil (~30 mm × 30 mm) was used for signal reception. After induction of anesthesia with 3% isoflurane, rats were placed in an MRI compatible cradle, and the head was fixed with ear bars and a support ring for the upper incisors in order to reduce movement artifacts. Animals were anesthetized with 2% isoflurane (Forane, Baxter, Deerfield, IL, USA) in a 70/30 mixture of N_20 and O_2, and vital functions were monitored during the whole anesthesia period using DASYLab (version 9.0, Measurement Computing Cooperation, Norton, MA, USA). The breathing rate was assessed *via* a breathing pillow, placed under the thorax, and kept at 70–80 breaths/minute by adjusting the isoflurane concentration. Body temperature was recorded with a rectal temperature probe, and regulated by a feedback system (set value: 37 °C) controlling a heating blanket with warm circulating water (Medres, Cologne, Germany).

T_2-weighted imaging (T2WI) was chosen for the anatomical detail of the images (first TE) and the information on tissue microstructure. Diffusion tensor imaging (DTI) was acquired for information on tissue anisotropy and myelination. Both scan protocols, T2WI and DTI, were set to cover the volume between olfactory bulb and cerebellum and were acquired with identical geometry (field of view: 28 mm × 28 mm, matrix 192 × 192, 0.5 mm slice thickness, no interslice gaps). The number of slices was adjusted individually in every session in order to account for brain growth.

T2WI was acquired using a Multi Slice Multi Echo sequence (MSME; TR/TE = 5000 ms/10 ms; 10 echoes with 10 ms inter-echo spacing). DTI was recorded with an 8-shot spin echo EPI sequence (30 directions; b-value = 630 s/mm^2, and five supplementary A_0 images) using a Stejskal–Tanner sequence.

The TurboRARE sequence, used for the generation of the rat brain template, used a TR/TE_{eff} = 4000 ms/32.5 ms and a RARE factor of 8. Two averages were recorded with a field of view 28 mm × 28 mm (matrix 192 × 192) and 0.5 mm slice thickness.

Postprocessing

Quantitative T_2 maps were calculated from the MSME multi-echo trains assuming mono-exponential decays, using IDL (IDL version 6.4, Boulder, CO, USA).

Raw diffusion data was first eddy current corrected (FSL version 4.1.7, FMRIB Centre, Oxford, UK). Then, eigenvalues (λ_1, λ_2, λ_3) and mean diffusivity (MD) maps were calculated using DTI Studio (DTI studio version 3.0.3, Baltimore, MD, USA). As the tensor elements have been reported to be more sensitive than the fractional anisotropy (FA) alone which is a mathematical expression of the combination of the tensor elements (Bockhorst et al., 2008; Deo et al., 2006; Song et al., 2002), we have focused our analysis on $\lambda_{\parallel}$and $\lambda_{\perp}$. The three eigenvalues stand for the length of the three principal axes (directions) measured in diffusion tensor imaging. The first, largest eigenvalue (λ_1) represents the axial or parallel diffusivity ($\lambda_{\parallel}$), while the perpendicular or radial diffusivity ($\lambda_{\perp}$) is the average of the two minor axes, the second (λ_2) and third eigenvalue (λ_3). The average of all three eigenvalues is the mean diffusivity (MD) (Basser et al., 1994).

Registration and VOIs

The registration paradigm included registration to a template brain. This template was generated by registering separate data sets of 35 three month-old male Wistar rats to each other. Then one average brain template was generated from these 35 registered data sets. Additionally, volumes of interest (VOIs) for several anatomical structures were manually created based on a rat brain atlas (Paxinos and Watson, 1998). In the following, the VOIs of the cortex and the striatum are analyzed. All analysis used the brain volume represented by the series of coronal sections shown in Fig. 1, where the volumes were conservatively selected to avoid errors at the boundaries of the acquired maps and thus in order to avoid an error in volume determination. The ROI "*whole brain*" was defined as the brain tissue limited caudally by the cerebellum and rostrally by the rhinal fissure, as demonstrated in the sagittal section scheme in Fig. 2.

First, the 3M MRI dataset was registered to the template brain, then, the 2M and 6M data sets were registered to the 3M data set of each subject, the 1M MRI data was registered to the 2M and the 3W data to that at 1M. Thus, data sets of all time points of each individual were registered step-by-step to the template brain starting with the data sets of the 3 month old animals and propagating to the next-closest time point. Using the information provided by the deformation field (see below for details) for each registration step, the template VOIs were propagated from one time point to the next, thereby enabling quantitative comparison of corresponding areas. Subsequently, the VOIs were evaluated quantitatively for MRI parameter changes and for volume change.

All registration steps were carried out with the first echo (TE1) image of the MSME sequence (TR/TE = 5000 ms/10 ms), chosen for its high anatomical details and high signal-to-noise ratio (SNR). Individual brain masks were created (brain extraction tool in FSL) and applied during all steps of the registration process. The masks of all, the reference data set and the deforming data set, were used to crop the images to sections merely larger than the masks themselves to facilitate the registration steps of the brain. The quality and success of the registration process was controlled by visual inspection using a custom-made graphic user interface (GUI) (Khmelinskii et al., 2013).

Registration was performed in a coarse-to-fine process. Initial registration was accomplished with a rigid transformation for rough global alignment. Subsequently, an affine registration was conducted to compensate for brain size scaling during the animal's developmental growth. Finally, a non-rigid B-spline registration was applied to follow regional changes. A Gaussian image pyramid was employed in all registration steps, applying four resolutions for the rigid and affine and two for the B-spline part. Normalized correlation was used as a similarity

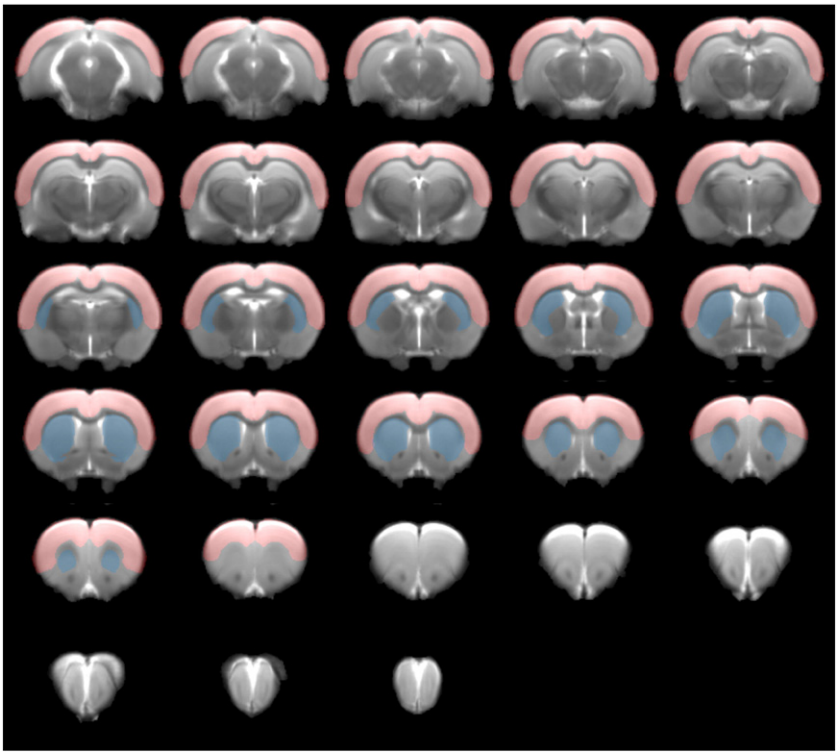

Fig. 1. Template brain with regions of interest (ROIs). The template brain is an average MR image stack (TurboRARE) of a three month old rat brain (n = 35 male Wistar rats). The extent shown here from the onset of the cerebellum caudally (top left) to the rhinal fissure rostrally (right bottom) was defined as the *whole brain* ROI. Superimposed are the structural ROIs for cortex (red) and striatum (blue), both based on Paxinos and Watson rat brain atlas (Paxinos and Watson, 1998).

metric. The registration was implemented using the open source image registration toolbox Elastix (Klein et al., 2010). Detailed information on the registration parameters can be found at the Elastix website (http://elastix.bigr.nl/wiki/index.php/Par0020).

The absolute three-dimensional deformation, necessary for the registration of two data sets, is contained in the deformation matrix. The identical geometry of the DTI and MSME (thus also the TE1) data sets allowed us to apply these deformation matrices of the TE1 images in a second step to the parameter maps. The VOIs are then available for all parameter maps of all time points, thereby enabling not only the quantitative evaluation of the T_2 and diffusivity changes, but also the computation of brain structure volumes.

Cortical thickness determination

The mean cortical thickness was assessed by measuring the distance between external capsule/corpus callosum and dorsal brain surface. For this purpose, a semi-automated macro was implemented in ImageJ (version 1.46, NIH, Bethesda, MD; USA) measuring the cortex thickness perpendicular to a manually generated outline of the white matter. In this procedure the most medial part of the corpus callosum was excluded, because the assumption of a parallel cortex is not met in this region.

In detail, in a first step a "profile image" is created: A manually generated outline ("Segmented Line" tool in ImageJ) is used to fit a curve to the center of the corpus callosum using Gaussian combined with Heaviside

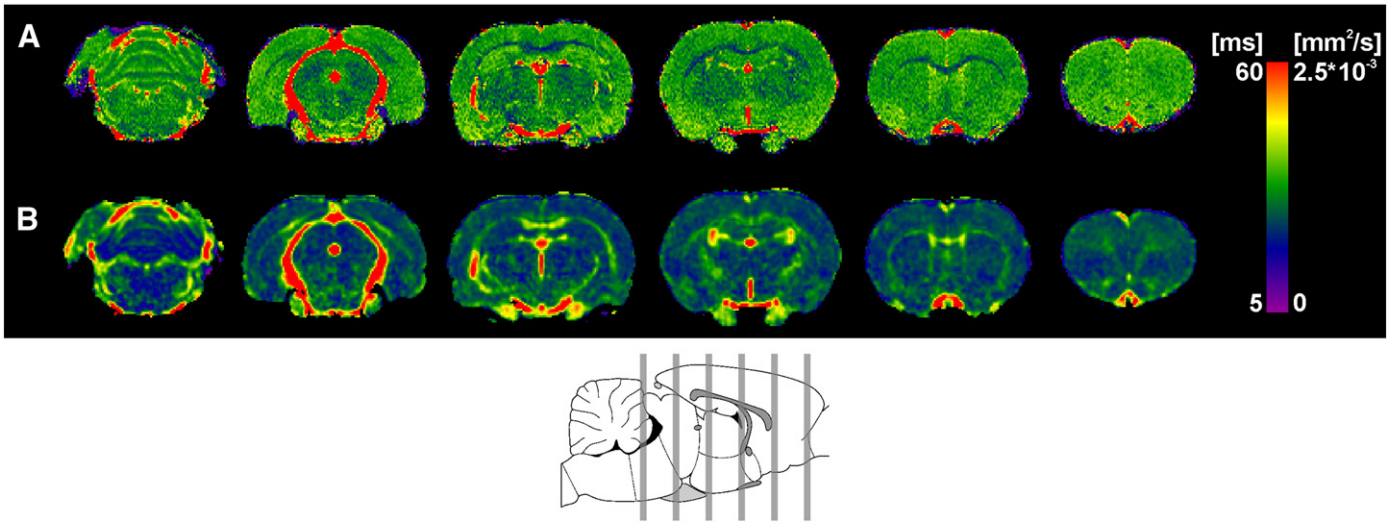

Fig. 2. Magnetic resonance data. Representative T_2 (A) and $\lambda_{\parallel}$ (B) map of a 3M old animal, before registration to the template brain. Depicted is every 5th MR image of an acquired 30 slice-stack, gray lines in the rat brain sketch (Paxinos and Watson, 1998) below indicate their anatomical position.

step function fits. Straight lines, perpendicular to this curve and reaching the cortical surface, form the "profile image", *i.e.* the curve is straightened. In a second step, the cortex thickness is measured in the profile image by determining the length of the straight lines perpendicular to the curve crossing the cortex only. This distinction is achieved by submitting the gray scales in the profile image to a Rodbard fitting function. This procedure of cortex thickness determination was performed for the somatosensory cortex in 5–6 slices.

Histology

At 3W, 3M and 6M, animals were sacrificed by transcardial perfusion with phosphate buffered solution (PBS) and 4% paraformaldehyde (PFA). Brains were postfixed overnight in 4% PFA before treatment with 30% sucrose. Tissue sections of 40 μm thickness were cut (Microtome, Leica Microsystems, Wetzlar, Germany) and preserved at −20 °C for histological staining. Sections at six selected levels were stained for both myelin and for cell nuclei, using Black-Gold II (BGII) (Schmued et al., 2008), and cresyl violet (CV), respectively (both: EMD Millipore, Billerica, MA, USA).

In order to assess the cell and myelin density in the brain, image acquisition and evaluation was conducted with a Keyence BZ9000 fluorescence microscope (Keyence, Neu-Isenburg, Germany) with a cell count analysis tool (Keyence). Quantification was based on contrast and color intensity in full-focus projections of images with 20× magnification (focal planes of 3 μm). ROIs were chosen in multiple areas: four cortical ROIs per hemisphere, each, in 6 sections (48 in total) and three striatal ROIs per hemisphere, each, in three sections (18 in total). Relative myelin content was defined as the relative area covered by BGII stained processes; cell density was determined as the number of CV stained cell nuclei per area.

Statistics

Longitudinal MRI data was evaluated using repeated measures ANOVA (SPSS version 18, IBM Corp. Armonk, NY, USA) with a repeated within-subject design. Where Mauchly's test indicated that the assumption of sphericity was violated ($p < 0.05$), we report the results with Greenhouse–Geisser corrected (ε) degrees of freedom and significance levels. Post-hoc pairwise comparisons with Bonferroni test are reported for consecutive time points only, unless interpretation of supplementary comparisons was useful.

Histological data was checked upon homogeneity of variances using Levene's test and analyzed with a one-way ANOVA with subsequent Bonferroni correction (SPSS).

All data were expressed as standard error of the mean (SEM) unless otherwise stated.

Results

Volume changes during development

The brain undergoes a strong growth during the first postnatal months. This growth curve was found to be quite homogeneous across the eight animals examined in this study. The volume change is significant for all three VOIs (whole brain: $\chi^2(5) = 16.7$ $p < 0.05$, $\varepsilon = 0.46$; $F(1.37,9.6) = 68.86$, $p < 0.001$; cortex: $F(3,21) = 65.48$, $p < 0.001$; striatum $\chi^2(5) = 18.3$ $p < 0.05$, $\varepsilon = 0.4$; $F(1.2, 8.4) = 33.5$, $p < 0.001$). Whole brain volume (excluding cerebellum and olfactory bulb) increases from $1202.9 +/- 18.9$ mm^3 (SEM) to $1585.5 +/- 43.9$ mm^3 (SEM) (Fig. 3A), thus gaining about 30% during the five weeks between postnatal week three and end of month two ($p < 0.001$). After 2M, brain volume is no longer changing significantly. Analyzing the cortical and striatal volumes separately, their volumetric plots (Figs. 3B and C), both show a highly significant increase ($p < 0.001$) from 3W to 1M, a continuous growth from 1M to 2M ($p < 0.05$), and no significant change from 2M to 3M.

Separate to the strong volume growth of whole brain, cortex and striatum, the cortical thickness shows a different developmental growth pattern. The cortical thickness grows substantially and significantly between 3W and 1M ($p < 0.05$), at which time it stabilizes already (Fig. 3D) ($\chi^2(5) = 14.96$ $p < 0.05$, $\varepsilon = 0.43$; $F(1.29,9) = 6.86$, $p < 0.05$).

Quantitative MRI parameter changes during development

Simultaneous with the dramatic volume changes, the quantitative MRI variables are changing. T_2 relaxation time of the whole brain, the cortex and the striatum decreases substantially and continuously in the time window between 3W and 2M ($p < 0.05$ between 3W/1M and 1M/2M) with a statistically significant effect over time (whole brain: $F(3,21) = 28.84$, $p < 0.001$; cortex: $F(3,21) = 36.4$, $p < 0.001$; striatum: $F(3,21) = 30.6$, $p < 0.001$). After 2M, the T_2 decrease in the striatum levels out, while the T_2 values of cortex and whole brain are still decreasing until the age of six months (Fig. 4A). Note that the T_2 decrease of the whole brain contains a contribution from shrinking relative ventricle volume, while the cortical and striatal T_2 decrease is primarily due to tissue reorganization processes.

The diffusion parameters axial ($\lambda_\parallel$), mean (MD), and radial diffusivity ($\lambda_\perp$) show a decrease during the first six months of cerebral development with a statistical effect over time (repeated measures ANOVA) in all three structures analyzed (Figs. 4B–D). However, not all parameters show differences between subsequent time points (*T*-test).

$\lambda_\parallel$ evolves similarly in cortex and striatum, both in respect to the absolute values and the relative change over time. In both areas, $\lambda_\parallel$ shows a light but steady decrease during the first three months (cortex: $F(3,21) = 6.72$, $p < 0.01$; striatum: $F(3,21) = 9.33$, $p < 0.001$) followed by stagnation thereafter. Mean $\lambda_\parallel$ of the whole brain is slightly higher compared to the absolute values of cortex and striatum, but follows the same qualitative developmental pattern ($F(3,21) = 6.86$, $p < 0.01$). None of the three structures shows a significant difference in $\lambda_\parallel$ between sequential time points, but they all show a difference between 3W and 3M ($p < 0.05$).

MD values of the three VOIs tend to increase from striatum to cortex to whole brain (Fig. 4C), though their qualitative development over time is alike and statistically significant in all three cases (whole brain: $F(3,21) = 13.29$, $p < 0.001$; cortex: $F(3,21) = 9.1$, $p < 0.001$, striatum: $F(3,21) = 19.13$, $p < 0.001$). The first three time points until 2M show a slowly decreasing trend followed by a steep decline between 2M and 3M and a rather stable phase thereafter (*i.e.* 3M to 6M). Despite the qualitative similarity in the development, the cortical ROI did not show any significant changes between sequential time points.

$\lambda_\perp$ development with time is similar to MD, but here the cortical values are equal to or even higher than those of the whole brain. In all three VOIs, an effect of time was observed (whole brain: $F(3,21) = 11.69$, $p < 0.001$; cortex: $F(3,21) = 6.72$, $p < 0.01$; striatum: $F(3,21) = 21.23$, $p < 0.001$) with a particularly strong $\lambda_\perp$ decrease between 2M and 3M. This difference was found to be significant in whole brain and striatum ($p < 0.05$), while in the cortex, the $\lambda_\perp$ values at 3M significantly differ only from 3W and 1M ($p < 0.01$) but not from 2M.

Histological analysis of developmental changes

Histological evaluation of the brains at different developmental stages revealed a pronounced increase in myelinated fibers on Black-Gold II staining during the first six months. This development was analyzed both qualitatively (Fig. 5) and quantitatively (Fig. 7A). The three-week young brains show positive staining only in the white matter structures, such as the corpus callosum, the anterior commissure, or fornix (Fig. 5). At 3W, myelinated fibers are barely detectable in the cortex, their contribution to the tissue is as low as 1% (Fig. 7A). By 3M, the radially oriented fibers of the cortex become myelinated to a high degree and cover about 15% of the cortex. At six months of age, the cortical

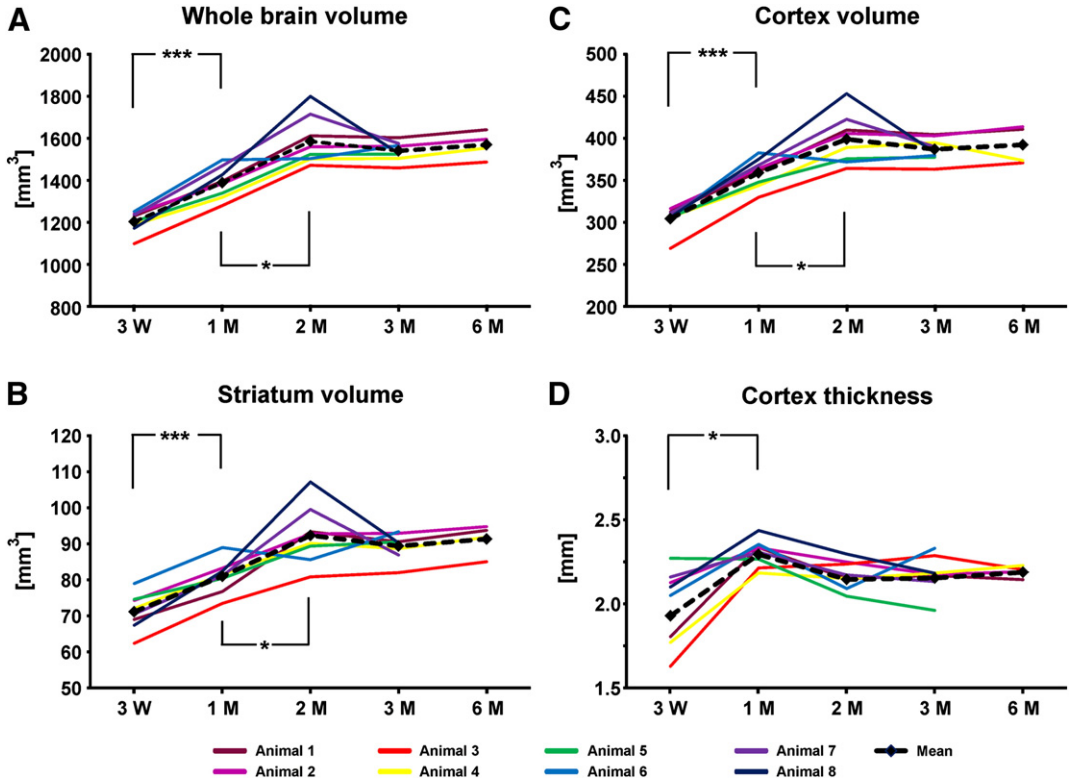

Fig. 3. Individual volume changes of developing brain regions. The graphs show the absolute volume of the whole brain (A), the striatum (B) and cortex (C) and the cortical thickness (D) plotted against the age for each individual animal. Here and in subsequent figures, ages are given as follows: three weeks, one, two, three and six months: 3W, 1M, 2M, 3M and 6M respectively. Red/yellow lines represent animals #1–4, which were followed from 3W to 6M, blue/green lines indicate animals #5–8, followed from 3W to 3M of age; the broken black line indicates the mean value. Note, for this and subsequent figures statistical significance is indicated for consecutive time points only; significance levels are Bonferroni corrected and represented by * $p < 0.05$, ** $p < 0.01$ and *** $p < 0.001$ and correspond in color to the respective data line.

layers can be recognized and at this time, 70% of the cortex is $BGII^+$. The increase of cortical $BGII^+$ area is apparent over time and found to be highly significant ($F(2,6) = 32,3$, $p < 0.001$).

In the striatum changes are not as pronounced upon visual inspection. Quantitative analysis, however, reveals a strong increase in relative area covered with myelin ($F(2,6) = 33,4$, $p < 0.001$). The white matter bundles of the striatum are already distinguishable at three weeks but make up only 5% of the area; with time they become more intensively stained and increase in numbers until, at three months, they represent about 28% of the striatal area. Here, in contrast to the cortical maturation, a further increase from 3M to 6M was not observed.

No maturation change is noticeable by visual inspection of CV staining of animals of different ages (Fig. 6). Quantitative analysis of cell density confirms this impression for the cortical but not for the striatal ROIs (Fig. 7B). Cell density in the cortex remains stable over the course of the first six months of maturation, with no distinct differences between the single time points. In the striatum, however, cell density is decreasing between 3W and 3M, reaching a constant level thereafter ($F(2,6) = 25.3$, $p < 0.01$).

Discussion

This study combined a longitudinal and cross-sectional approach to monitor postnatal development in Wistar rats by noninvasive *in vivo* MRI and conventional histology. We have assessed the noninvasive *in vivo* biomarkers cerebral growth, tissue water and tissue structure by MRI relaxation time measurements, and tissue diffusion parameters together with *ex vivo* tissue myelination state and cell density. With these parameters, we have been able to characterize and define the time window of brain maturation in the male Wistar rat. This novel definition is of paramount importance for longitudinal studies of the rat brain when it is important to discriminate in which phase of development or maturation the subject under investigation is at the start of the study or during its runtime. We have shown in this study that the rat brain and especially the rat brain cortex are indeed not yet fully developed at 3 months of age. Furthermore, individual brain regions and processes have been shown to have individual time scales for maturation. Based on these observations, we recommend careful examination of the brain structures under investigation before investigating functional topics or disease models in longitudinal examinations.

In vivo MRI parameter patterns of brain maturation

When inspecting the *in vivo* data alone, different maturation time profiles become apparent. Changing MR parameters alone, however, do not allow conclusions about single microstructural processes. Yet, the combination of the different *in vivo* measurements in this study suggested cell density and myelination to be strongly responsible for changes in T_2 and diffusion, respectively. Additional histological tissue characterization can reveal such changes in microstructure with high sensitivity, thus permitting unambiguous interpretation of the MRI parameters. In the present study, two tissue properties were analyzed: the development of myelinated fibers was visualized with the well characterized Black-Gold II staining (Schmued et al., 2008), while cell density was evaluated with cresyl violet, in order to detect neuronal as well as glial cell types.

Independent of ROI selection (whole brain, cortex or striatum), the first two months show continuous volume changes, accompanied by a dramatic T_2 decrease. This result of decreasing T_2 relaxation time with early growth is supported by an earlier study on postnatal rats in our group (Kallur et al., 2011). Judging from the T2WI-based volume data alone, one is tempted to believe that brain growth is completed by the end of two months. Interestingly enough, we have found that the quantitative parameter, T_2 relaxation time, continues to decrease beyond 2M,

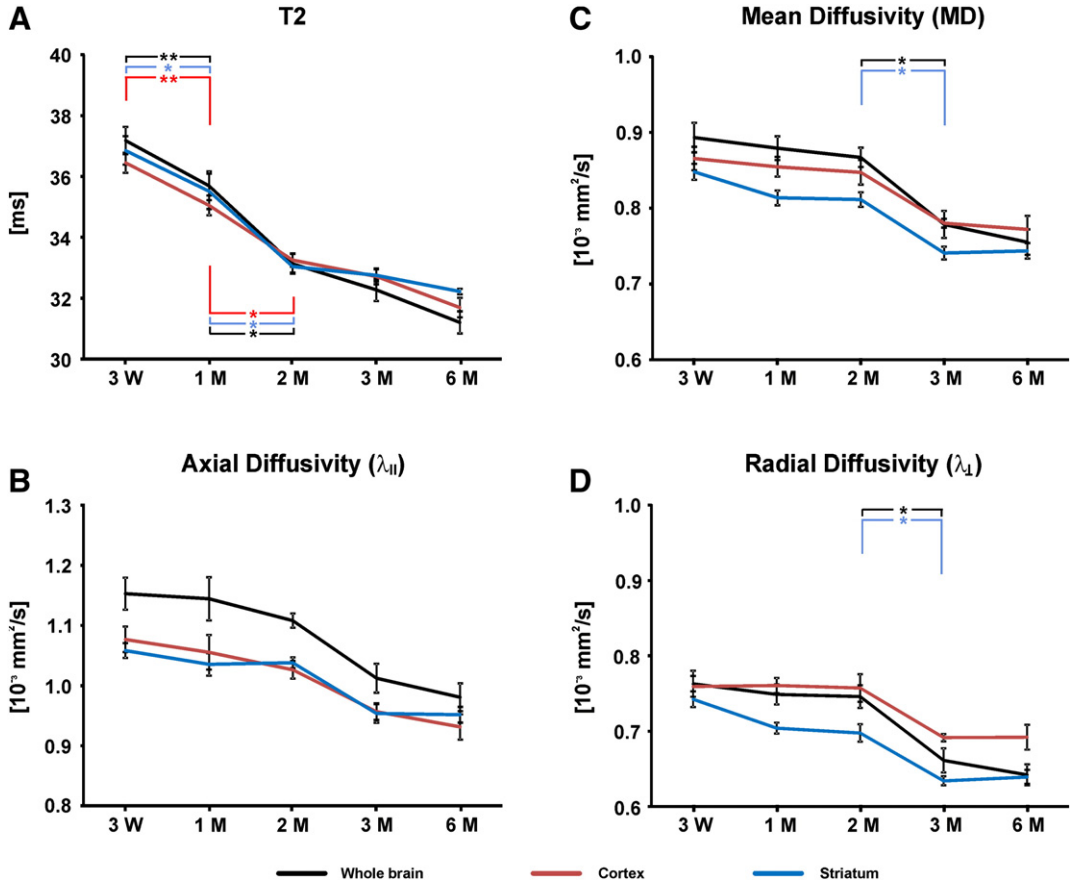

Fig. 4. Quantitative MR parameters. Evolution of the mean T_2 (A), axial (B), mean (C) and radial diffusivity (D) over time is shown for the three regions of interest: whole brain (black), cortex (red) and striatum (blue). The data shown is an average of n = 8 rats until 3M and n = 4 rats at 6M of age with error bars indicating the standard error of the mean (SEM).

indicative that water content and/or tissue reorganization processes continue to change at a time when the brain volume has reached a mature state. This is in agreement with reports on dramatic decrease of brain water content with increasing gestational age in humans (Hüppi and Dubois, 2006), while it continues to further decrease substantially during early development for many species, including rodents (Samorajski and Rosten, 1973). This T_2 decrease (as an indicator of brain water content decrease) may well be related to increasing myelination as a growing tissue compartment, consequently resulting in decrease of the extracellular space available for brain water.

Myelination as well as increased cell density, both decrease the amount of free water in the brain in favor of intracellular water compartmentation (Anderson et al., 2000; Chabert and Scifo, 2007). This is in agreement with early neurochemical studies (Fuller et al., 1982; Lancaster et al., 1984; Norton and Poduslo, 1973) which had reported that brain development is accompanied by a decreasing water content of the tissue and a constant increase of the myelin fraction. Indeed, our diffusion data show that the myelination process is not yet finished at 2M, again in agreement with the early reports describing ongoing myelination increases in healthy rats during their observation period of 52 days (Lancaster et al., 1984) and 70 days (Fuller et al., 1982), respectively. Previous studies reported that during adolescence changes in DTI parameters reflect myelination, but during the neonatal period, they rather reflect changes in general water content and structure (Wozniak and Lim, 2006). In our study, a pronounced decrease in the DTI parameters MD and $\lambda_\perp$ was found between 2M and 3M and reflects the dramatic change of the myelination status, confirmed by histology across the whole brain *ex vivo* between 3W and 3M (Figs. 5 and 7). As discussed earlier in model systems, diffusion anisotropy integrates information on myelination state and on axonal structure (Deo et al., 2006; Song et al., 2002). According to these authors, myelination changes are best represented by the radial diffusion tensor eigenvalue $\lambda_\perp$, while these changes have relatively little effect on the maximal eigenvalue $\lambda_\parallel$. Myelination acts like a restriction on radial free water mobility and, in consequence, leads to a reduced mean diffusivity, most clearly seen in a strong reduction in $\lambda_\perp$. This is in line with our MRI and histology results, showing that in the striatum with its strongly myelinated, big fiber bundles, MD as well as $\lambda_\perp$ are reduced more strongly than in the cortex. The drop in $\lambda_\parallel$ observed here is probably a result of the general diffusivity reduction, rather than actual reduced axial weighting. Though the *ex vivo* data is available only for 3W and 3M, the high temporal resolution of the DWI data suggests that the major period of myelination is between 2M and 3M.

When interpreting myelination, as assessed here by BGII staining, one must consider that staining intensity is not taken into account for the present quantification approach, thus denser packing in bundles is not represented in the evaluation. The strong myelination of the first three months is followed by rather subtle changes, observed both in staining intensity and stained area. In contrast to the DWI results, this is indicative that the brain is not completely developed at three months, thereby revealing the sensitivity limit of diffusion MRI.

In the following we discuss *in vivo* as well as *ex vivo* data of the different cerebral structures, followed by a recommendation for age-relevant brain studies.

Whole brain

The whole brain ROI shows higher MD and $\lambda_\parallel$ values and a stronger decrease over time, when compared to cortical and striatal ROIs. As the whole brain ROI includes all cerebral structures between olfactory bulb and cerebellum, it consists to a better part of white matter rich structures such as the hippocampus, the striatum, and the actual

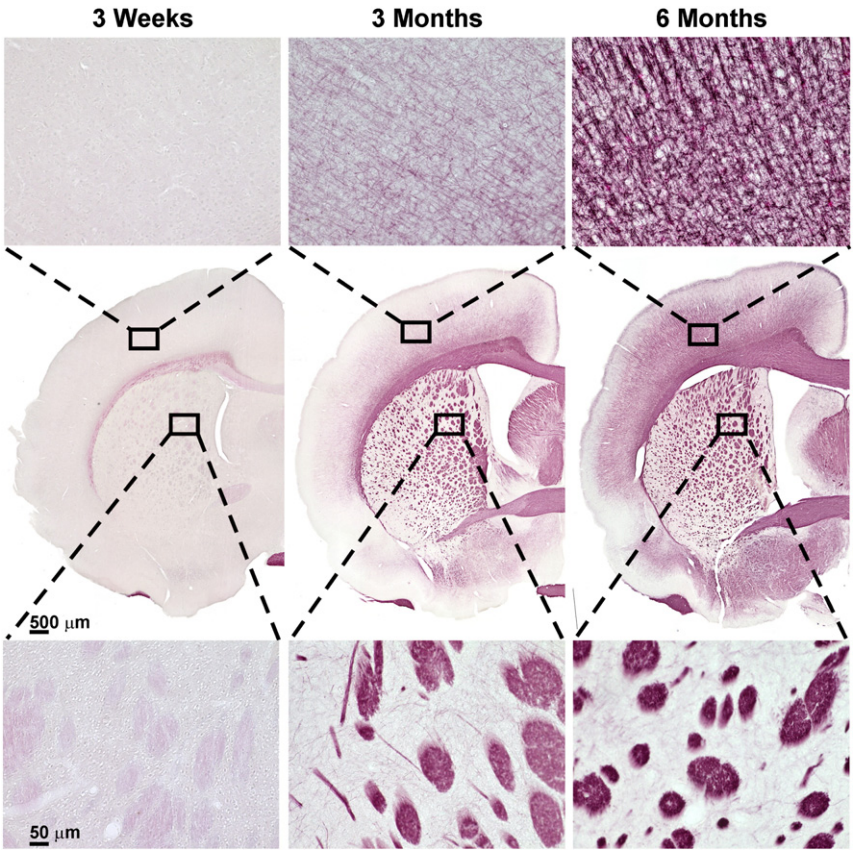

Fig. 5. Histological evaluation of myelin content. Black-Gold II staining was used to visualize cerebral myelin content, representative brain sections of differently aged animals are pictured here from left to right: 3W, 3M, 6M. The middle row shows an overview (4× magnification) of one hemisphere with the position of the two close-ups indicated by the black squares: the upper row shows a ROI (20×) in the cortex, the lower row in the striatum.

white matter. Thus, when interpreting the strong drop in diffusivity values with age, the major cause probably is myelination. As fluid compartments have the highest diffusivity, reduction in the relative size of the ventricles will further lower the mean diffusivity in the whole brain.

Cortex

The *ex vivo* and *in vivo* results for the cortical ROI suggest a rather complex maturation process. Most prominent is the apparent discrepancy between the evolution of cortical volume and of cortical thickness and of MRI diffusivity parameters and myelin content. These apparently contradicting findings reflect only different aspects of the same processes.

The cortical volume was found to increase until 2M, yet the cortex thickness has reached maximum already after 1M. These findings are in full accordance with *ex vivo* examination by Romand and colleagues, reporting a significant cortex increase along the long body axis between postnatal day 36 and 60 while thickness development already ended with postnatal day 36 (Romand et al., 2011). Thus, the cortex reaches its final thickness after one month while rostral/caudal expansion of the brain continues until at 2M.

Interestingly, the cortical growth phase is not accompanied by changes in cell density; according to Mortera et al. (Mortera and Herculano-Houzel, 2012), mainly neurogenesis rather than gliagenesis accounts for the volume increase. With the volume increase, the T_2 is reducing strongly until 2M, showing a decreasing trend afterwards. Apparently this T_2 change is not due to a changing density of cells, but must emerge from other maturation processes. A reduced T_2, as well as MD can indicate a reduction of free water in the tissue (Whittall et al., 1997), thus, decreasing the random movement of free water molecules and resulting in altered spin–spin interaction, the physical mechanism of T_2. Apart from myelination and higher cell density, the observed T_2 decrease may have several additional reasons coming from neuronal ramification and synaptogenesis, to simple compression and fine changes such as changing protein composition of the extracellular matrix. Especially the T_2 change beyond 3M, during growth stagnation and with major myelination processes terminated, reflects the high sensitivity of T_2 for tissue composition changes.

Our histological evaluation does not account for such processes of microscopic tissue composition alterations, so that *ex vivo* explanations for cortical T_2 changes are limited to the aspect of myelination. The BGII staining revealed a continued cortical myelination at least until 6M, contributing to reduction of extracellular space because of constant cell density. Although the radial organization increases pronouncedly on the BGII staining between 3M and 6M, this is not reflected on diffusion parameters. No decrease in either $\lambda_\perp$ or MD could be detected between these time points, indicating that further myelination after 3M was accompanied by other processes diminishing the radial diffusivity sensitivity. This diminishing diffusion sensitivity parallel to the ongoing myelination process may, at least in part, account for the apparent discrepancy between our results and earlier reports by Bockhorst and colleagues, reporting a decrease between postnatal day eight and 28, but no further change in cortical $\lambda_\parallel$, $\lambda_\perp$ or MD after postnatal day 28 (Bockhorst et al., 2008). Those earlier data may suffer from technical reduction of diffusion sensitivity: while we recorded our diffusion data at 11.7 T, data by Bockhorst et al. were collected at 7 T and needed more signal averaging, thus resulting in longer scan time, and, in consequence, making the images prone to movement artifacts which may lead to some blurring of the diffusion strength in the reconstructed quantitative parameter images. Support for such explanation comes from those authors reporting that the diffusion-weighted images needed to be

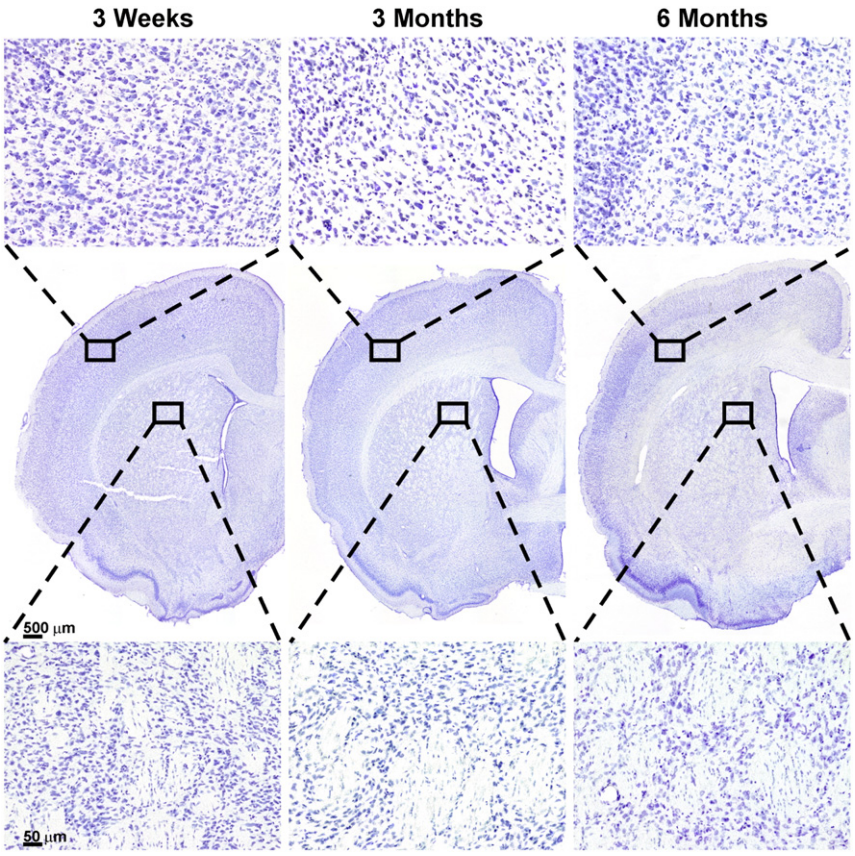

Fig. 6. Histological evaluation of cell density. Cell density was assessed *via* cell counting in cresyl violet stained sections. Representative brain sections of differently aged animals are pictured here from left to right: 3W, 3M, 6M. The middle row shows an overview (4× magnification) of one hemisphere, the upper and lower row show the close-ups indicated by the black squares: the upper row a ROI (20×) in the cortex, the lower row in the striatum.

warped to minimize image distortions induced by eddy currents. We therefore believe that our observations of diffusion changes persisting until 3M are based on more robust and more sensitive raw data recording.

The cortical architecture features radial compartments, like the pyramidal axons and functional columns, and layers perpendicular to the radial compartments. From such well characterized cortices as the primary visual cortex, it is known that the radial organization of the pyramidal neurons is established prenatally, and that their processes mature within the first postnatal weeks (Miller, 1986). This columnar/radial organization is not yet reflected in the histological staining, as the axons are not yet myelinated, but can be found in the DWI when inspecting the direction of the first eigenvector, $\lambda_{\parallel}$(Hoehn-Berlage et al., 1999). With the maturation of the cortical layers and the branching of the neurons within, the distinct and homogeneous pattern of the eigenvector dissolves, becoming less regular with increasing age. Though the radial structure appears dominant in the BGII staining, the layering structure of the cortex seems to modulate the major λ values seen in the DWI data afterwards. Cell-dense layers like layer IV, rich on interneurons, branches and cross connections, will have a more

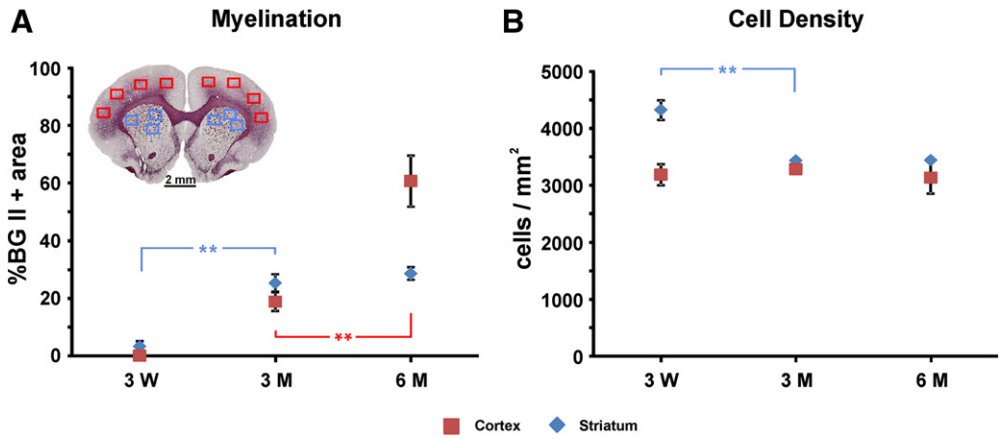

Fig. 7. *Ex vivo* histological quantification. Quantification of the histological sections was performed on eight cortical and six striatal close ups with 20× magnification per section. A representative overview section (4×) is inserted in the upper left, with the 14 ROIs indicated by red (cortex) and blue (striatum) boxes. The relative $BGII^{+}$ area reflects the extent of myelination (A), while cell density is assessed by the mean number of cells per mm^2 (B). Both graphs give the mean value for cortex (red) and striatum (blue) with error bars representing SEM ($n = 3$).

restricted and less directed diffusion than layers with fewer cell bodies. Though the spatial resolution is not sufficient to illustrate these differences within the cortex, diffusion of water molecules could be deflected between layers rather than along the myelinated axons in some parts of the cortex and be generally reduced during the maturation of the cortical parenchyma.

Striatum

In the striatum the developmental time scale observed in DWI appears to be consistent with the myelination process visualized in histology, showing big fiber bundles on CV and BGII stained tissue sections. The significant volume growth until 2M and the increasing trend until 6M are accompanied by an antiparallel development of the T_2 values equivalent to those in the cortex and whole brain ROIs. The changes in diffusivity are manifested quite strongly until 3M, as the striatum is rich in white matter bundles stretching toward the internal capsule. Histological assessment shows that in the same time frame, until 3M, cell number and myelin content of the striatum are changing remarkably and stabilize thereafter. Cell density is decreasing between 3W and 3M, maybe due to both, the striatal growth (until 2M) and the volume demanding myelination process. The strong myelination is reflected in the decrease of radial and mean diffusivity between 2M and 3M. At three months, however, all processes seem to be terminated and the striatal tissue has completely matured.

Consequences for investigations on cerebral disease models

Many studies on cerebral diseases are based on the assumption of inducing the disease or lesion on healthy and adult animals. There is, however, a wide body of literature on such disease model investigations using rats of body weight ranging between 270 and 320 g. According to standard weight-age diagrams provided by the animal suppliers for the strain of Wistar rats used in the present study, this weight range makes the animals typically around two months old, at any rate clearly younger than 3 months of age. In this case, volume change and cortical thickness have already stabilized, cell density in the striatum has also stabilized but myelination in both, striatum and cortex, continues up to 3M for striatum, for cortex even up to 6M. Based on the diffusion changes alone, myelination changes are very pronounced between months two and three. Taken these new observations together, it must be cautioned that lesion studies during this age period may be influenced by ongoing developmental brain maturation processes. This situation may be even more complex in the case of studies dealing with evaluation of therapeutic strategies. In light of our new observations, it would therefore be preferable to perform such disease model investigations (including those on therapeutic evaluations) on Wistar rats being at least three months of age at the beginning of the investigations.

Future studies will increase the temporal resolution of the maturation and growth changes to even better define the end of the developmental phase. Improvement of spatial resolution of the MRI will permit detailed analysis of structures prone to contain partial volume effects, such as corpus callosum or ventricular spaces, and will extend the whole volume to include hindbrain and olfactory bulb.

Conclusions

Combining longitudinal MRI measurements with histological tissue characterization, we have derived a temporal profile of postnatal rat brain maturation. Different cerebral structures show an individual timeline for postnatal development. While the striatum seems to be fully matured by three months, the cortex is still changing until at least six months. Our present results convincingly demonstrate that brain volume is a reliable variable of having reached a steady state situation concerning organ expansion while measurement of cortical thickness will be misleading for two to three month old rats. Clear indications of ongoing developmental changes in the rat brain point to the time window until three months of age; in particular persistent myelination aspects in cortex and striatum make it advisable to speak of “adult animals” only from three months of age on. Future investigations on disease models or lesions may have to consider this age of three months as a safer threshold to avoid ongoing developmental changes in the brain opposing the study of the patho-mechanisms of interest.

Acknowledgment

We gratefully acknowledge the support of Dr. Daniel Kalthoff for the development of the rat brain template based on MRI and his help with setting up ImageJ based macros for analysis of cortical thickness. We furthermore thank Melanie Nelles and Ulla Uhlenküken for their technical support. Financial support was obtained from the German Ministry of Education and Research (BMBF-0314104/Biomarkers of Brain Ageing) and from the EU FP7 program TargetBraIn (HEALTH-F2-2012-279017).

Conflict of interest

The authors have no conflict of interest. The funding agencies had no influence on study design, performance or analysis.

References

Andersen, S.L., 2003. Trajectories of brain development: point of vulnerability or window of opportunity? Neurosci. Biobehav. Rev. 27, 3–18.
Anderson, A.W., Xie, J., Pizzonia, J., Bronen, R.A., Spencer, D.D., Gore, J.C., 2000. Effects of cell volume fraction changes on apparent diffusion in human cells. Magn. Reson. Imaging 18, 689–695.
Basser, P.J., Mattiello, J., Lebihan, D., 1994. Estimation of the effective self-diffusion tensor from the NMR spin-echo. J. Magn. Reson. B 103, 247–254.
Bockhorst, K.H., Narayana, P.A., Liu, R., Vijjula, P.A., Ramu, J., Kamel, M., Wosik, J., Bockhorst, T., Hahn, K., Hasan, K.M., Perez-Polo, J.R., 2008. Early postnatal development of rat brain: *in vivo* diffusion tensor imaging. J. Neurosci. Res. 86, 1520–1528.
Chabert, S., Scifo, P., 2007. Diffusion signal in magnetic resonance imaging: origin and interpretation in neurosciences. Biol. Res. 40, 385–400.
Deo, A.A., Grill, R.J., Hasan, K.M., Narayama, P.A., 2006. *In vivo* serial diffusion tensor imaging of experimental spinal cord injury. J. Neurosci. Res. 83, 801–810.
Fuller, G.N., Divakaran, P., Wiggins, R.C., 1982. The effect of postnatal caffeine administration on brain myelination. Brain Res. 249, 189–191.
Hoehn-Berlage, M., Eis, M., Schmitz, B., 1999. Regional and directional anisotropy of apparent diffusion coefficient in rat brain. NMR Biomed. 12, 45–50.
Hüppi, P.S., Dubois, J., 2006. Diffusion tensor imaging of brain development. Semin. Fetal Neonatal Med. 11, 489–497.
Kallur, T., Farr, T.D., Boehm-Sturm, P., Kokaia, Z., Hoehn, M., 2011. Spatio-temporal dynamics, differentiation and viability of human neural stem cells after implantation into neonatal rat brain. Eur. J. Neurosci. 34, 382–393.
Khmelinskii, A., Mengler, L., Kitslaar, P., Staring, M., Hoehn, M., Lelieveldt, B.P.F., 2013. A visualization platform for high-throughput, follow-up, coregistered multicontrast MRI rat brain data. Proc. SPIE 8672, 86721W-86721W-7.
Klein, S., Staring, M., Murphy, K., Viergever, M.A., Pluim, J.P.W., 2010. elastix: a toolbox for intensity-based medical image registration. IEEE Trans. Med. Imaging 29, 196–205.
Lancaster, F.E., Philipps, S.M., Patsalos, P.N., Wiggins, R.C., 1984. Brain myelination in the offspring of ethanol-treated rats: *in utero versus* lactational exposure by cross-fostering offspring of control, pairfed and ethanol-treated dams. Brain Res. 309, 209–216.
Meaney, M.J., Stewart, J., 1981. A descriptive study of social development in the rat (Rattus norvegicus). Anim. Behav. 29, 34–45.
Miller, M.W., 1986. Maturation of rat visual cortex. III. Postnatal morphogenesis and synaptogenesis of local circuit neurons. Dev. Brain Res. 25, 271–285.
Mortera, P., Herculano-Houzel, S., 2012. Age-related neuronal loss in the rat brain starts at the end of adolescence. Front. Neuroanat. 6 (45). http://dx.doi.org/10.3389/fnana 2012.00045.
Norton, W.T., Poduslo, S.E., 1973. Myelination in rat brain: changes in myelin composition during brain maturation. J. Neurochem. 21, 759–773.
Paxinos, G., Watson, C., 1998. The Rat Brain in Stereotaxic Coordinates, 4 ed. Academic Press, San Diego, CA.
Romand, S., Wang, Y., Toledo-Rodriguez, M., Markram, H., 2011. Morphological development of thick-tufted layer V pyramidal cells in the rat somatosensory cortex. Front. Neuroanat. 5.5. http://dx.doi.org/10.3389/fnana 2011.00005.
Samorajski, T., Rosten, C., 1973. Age and regional differences in the chemical composition of brains of mice. Monkeys and Humans. Progress in Brain Research: Neurobiological Aspects of Maturation and Aging.Elsevier 253–265.

Schmued, L., Bowyer, J., Cozart, M., Heard, D., Binienda, Z., Paule, M., 2008. Introducing Black-Gold II, a highly soluble gold phosphate complex with several unique advantages for the histochemical localization of myelin. Brain Res. 1229, 210–217.

Song, S.K., Sun, S.W., Ramsbottom, M.J., Chang, C., Russell, J., Cross, A.H., 2002. Dysmyelination revealed through MRI as increased radial (but unchanged axial) diffusion of water. Neuroimage 17, 1429–1436.

Spear, L.P., 2000. The adolescent brain and age-related behavioral manifestations. Neurosci. Biobehav. Rev. 24, 417–463.

Spear, L.P., Brake, S.C., 1983. Periadolescence: age-dependent behavior and psychopharmacological responsivity in rats. Dev. Psychobiol. 16, 83–109.

Whittall, K.P., Mackay, A.L., Graeb, D.A., Nugent, R.A., Li, D.K.B., Paty, D.W., 1997. *In vivo* measurement of T2 distributions and water contents in normal human brain. Magn. Reson. Med. 37, 34–43.

Wozniak, J.R., Lim, K.O., 2006. Advances in white matter imaging: a review of *in vivo* magnetic resonance methodologies and their applicability to the study of development and aging. Neurosci. Biobehav. Rev. 30, 762–774.